Annales
Geophysicae

Open Access

EGU

The fate of O$^+$ ions observed in the plasma mantle:
particle tracing modelling and cluster observations

Audrey Schillings[1,2], **Herbert Gunell**[3,4], **Hans Nilsson**[1,2], **Alexandre De Spiegeleer**[3], **Yusuke Ebihara**[5],
Lars G. Westerberg[6], **Masatoshi Yamauchi**[1], **and Rikard Slapak**[7]

[1]Swedish Institute of Space Physics, Kiruna, Sweden
[2]Division of Space Technology, Luleå University of Technology, Kiruna, Sweden
[3]Department of Physics, Umeå University, Umeå, Sweden
[4]Belgian Institute for Space Aeronomy, Brussels, Belgium
[5]Research Institute for Sustainable Humanosphere, Kyoto University, 611-0011, Gokasho, Uji, Kyoto, Japan
[6]Division of Fluid- and Experimental Mechanics, Luleå University of Technology, Luleå, Sweden
[7]EISCAT Scientific Association, Kiruna, Sweden

Correspondence: Audrey Schillings (audrey.schillings@irf.se)

Abstract. Ion escape is of particular interest for studying the evolution of the atmosphere on geological timescales. Previously, using Cluster-CODIF data, we investigated the oxygen ion outflow from the plasma mantle for different solar wind conditions and geomagnetic activity. We found significant correlations between solar wind parameters, geomagnetic activity (K_p index), and the O$^+$ outflow. From these studies, we suggested that O$^+$ ions observed in the plasma mantle and cusp have enough energy and velocity to escape the magnetosphere and be lost into the solar wind or in the distant magnetotail. Thus, this study aims to investigate where the ions observed in the plasma mantle end up. In order to answer this question, we numerically calculate the trajectories of O$^+$ ions using a tracing code to further test this assumption and determine the fate of the observed ions. Our code consists of a magnetic field model (Tsyganenko T96) and an ionospheric potential model (Weimer 2001) in which particles initiated in the plasma mantle region are launched and traced forward in time. We analysed 131 observations of plasma mantle events in Cluster data between 2001 and 2007, and for each event 200 O$^+$ particles were launched with an initial thermal and parallel bulk velocity corresponding to the velocities observed by Cluster. After the tracing, we found that 98 % of the particles are lost into the solar wind or in the distant tail. Out of these 98 %, 20 % escape via the dayside magnetosphere.

1 Introduction

Before the 1970s, it was believed that the solar wind was the primary source of magnetospheric plasma. However, this conception became obsolete a few years later with the studies of Shelley et al. (1976) and Sharp et al. (1977), who observed ionospheric O$^+$ ions with high velocities in the high-latitude ionosphere. A few decades later, it is now well known that ion upflow from the ionosphere is a significant source for the magnetosphere (Hoffman, 1968; Chappell et al., 1987; Abe et al., 1993), and it is accelerated through several processes to reach the high-altitude cusp and plasma mantle. A part of this ion upflow is also known as the polar wind, in analogy with the solar wind (Axford, 1968). The polar wind is composed of H$^+$, He$^+$, O$^+$, and electrons with an energy of a few eV and commonly observed between 1000 km and roughly 50 000 km. Polar wind observations have been reviewed by Yau et al. (2007). At higher altitudes, the ionospheric composition changes, and consequently the terminology of polar wind (including several species) is replaced by ionospheric outflow, which includes only one species. Furthermore, the ion outflow is then divided into two distinct populations, cold ions (up to a few tens of eV) and hot ions (up to a few tens of keV). The cold ions – detected with the spacecraft wake technique (Engwall et al., 2009) – are believed to be dominant for the magnetospheric plasma (An-

dré and Cully, 2012). These ions have been observed in the lobes (Haaland et al., 2009, 2012; Liao et al., 2010), have low enough parallel velocity so that convection dominates, and therefore will likely end up in the plasma sheet during strong solar wind conditions and a southward interplanetary magnetic field (IMF) (Haaland et al., 2012). Under a northward IMF the convection is more stable and weaker (Haaland et al., 2012), meaning this cold population will escape in the distant tail and be lost into the solar wind. The energetic ions are frequently heated transversely to the magnetic field due to wave–particle interactions in the cusp (Norqvist et al., 1998; Strangeway et al., 2005; Slapak et al., 2011; Waara et al., 2011; Nilsson et al., 2012) and parallel to the magnetic field due to magnetic mirror force, parallel electric field, or centrifugal acceleration (Nilsson et al., 2008; Nilsson, 2011). Arvelius et al. (2005) showed that O$^+$ ions are accelerated from less than 0.1 keV to more than 1 keV between 8 and 12 Re. The authors suggested that wave–particle interaction plays the main role in the ion heating and subsequent acceleration. These energetic ions form the ion outflow at higher altitudes, and several studies demonstrate the correlation between energetic ion outflow and solar and solar wind conditions (e.g. Peterson et al., 2001; Kistler et al., 2006; Kistler and Mouikis, 2016; Li et al., 2012; Schillings et al., 2019). It is the presence of a cusp and a polar cap that makes magnetised planets have atmospheric escape rates at least as high as planets without intrinsic magnetic fields (Gunell et al., 2018).

The main route of outflowing/escaping energetic ions is along open magnetic field lines, which include the polar cap, cusp, and plasma mantle. The polar cap is defined as the footprint of the open magnetic field lines and the cusp as the entry of the solar wind into the magnetosphere. The plasma mantle is the region downstream of the cusp formed by reflected particles from the cusp, which are then convected toward the tail (Rosenbauer et al., 1975). Using DE data at mid-altitude far below the plasma mantle, Yau et al. (1985, 1988) studied the dependency of the O$^+$ outflow in the polar cap and the auroral zone on the geomagnetic activity (K_p) and the EUV flux (F10.7 index). At the solar maximum, they found about 1 order of magnitude increase for the O$^+$ and H$^+$ outflow between active ($3 \leq K_p \leq 5$) and quiet time ($K_p \leq 2$). Similarly at higher altitude, Slapak et al. (2017) studied the O$^+$ outflow in the plasma mantle and dayside high-latitude magnetosheath for different geomagnetic conditions using the K_p index. In these regions, the flux is high, indicating that a large part of outflowing ions at DE altitude reaches the Cluster altitude rather then entering the near-Earth plasma sheet. They found that the O$^+$ escape rate increases by 1.5 orders of magnitude during very disturbed magnetospheric conditions ($K_p \geq 6$) compared to quiet conditions ($_{Kp} \simeq 0$–2). Despite 5 years of data, Slapak et al. (2017) did not have enough statistics for extreme disturbances, and therefore Schillings et al. (2017, 2018) performed case studies of major geomagnetic storms ($K_p \geq 7+$) in order to complement the study of Slapak et al. (2017). The authors found a 2 orders of magni-

tude enhancement in the O$^+$ outflow for the major storms as compared to the average O$^+$ flux for the same year of each storm. They also suggested that the O$^+$ ions have been heated enough when they reach the plasma mantle to eventually escape the magnetosphere. During major geomagnetic storms Slapak and Nilsson (2018) estimated a perpendicular velocity of the plasma mantle O$^+$ to 35 km s^{-1} and a parallel velocity of 115 km s^{-1}; thus, for their particular example the ions would reach the plasma sheet around -50 Re. As the near-Earth X line is pushed towards Earth during disturbed conditions, these ions are expected to escape into the distant tail.

Models and simulations have been extensively employed to investigate polar wind and ionospheric outflow. Schunk and Sojka (1989) simulated the polar wind behaviour using a combination of a low-altitude ionosphere–atmosphere and a high-altitude hydrodynamic model in a simulated region from 120 to 9000 km. They discovered the complexity of the polar wind density structures in different altitude ranges as well as for geomagnetic variations. Polar wind behaviour during one idealised geomagnetic storm has been investigated by Schunk and Sojka (1997), who updated their model to an altitude coverage of 90 to 9000 km for latitudes higher than 50°. They investigated the seasonal and solar cycle variations for four idealised geomagnetic storms (winter and summer solstices and solar minimum and maximum). They found that O$^+$ upflow increases over the polar cap during the storms, while O$^+$ is the dominant ion species at all polar latitudes. These results are similar to the ones by Barakat and Schunk (2006), who studied the generalised behaviour of the polar wind, also during an idealised geomagnetic storm using a macroscopic PIC (particle-in-cell) model. Their results agreed with satellite observations. At an intermediate lower altitude of 4000 km, Horwitz et al. (1994) determined the bulk velocity and temperature profiles of O$^+$ and H$^+$ in the polar wind using a semi-kinetic outflow model. They found that centrifugal forces increase the outflowing O$^+$ flux by 2 orders of magnitude when the convection electric field is enhanced from 0 to 100 mV m^{-1}. A similar result has been shown by Abudayyeh et al. (2015), who used a Monte Carlo simulation based on the Tsyganenko T96 model and included the effects of the ambipolar electric field as well as gravitational and mirror forces. Additionally, Abudayyeh et al. (2015) observed higher bulk velocities and densities (H$^+$ and O$^+$) in the cusp than in the polar cap.

At an altitude range of 1.2 to 15.2 Re, Barghouthi et al. (2016) employed the same 1-D Monte Carlo model used by Abudayyeh et al. (2015) to investigate energetic H$^+$ and O$^+$ outflows along two trajectories (from the polar cap to the cusp) and compared them with Cluster data. Considering the centrifugal acceleration, the ambipolar electric field, and the wave–particle interaction, they concluded that the latter was the most important mechanism, especially at higher altitudes (cusp). Finally, a statistical model of the fate of energetic ions showed that these ions are highly dependent on the

magnetic field configuration. Therefore, for a quiet magnetic field, more ions escape directly through the magnetopause, whereas for an active magnetic field, the ions are convected towards the tail and reach the distant tail at 50 Re (Ebihara et al., 2006). Ebihara et al. (2006) also showed that under strong convection most of the ions in their model end up in the ring current.

Models about the polar wind and ion outflow behaviour already exist. These models take into account different altitudes and include the heating processes the ions are subject to. Ebihara et al. (2006) discussed the fates of the ions launched at different magnetic local times (MLTs) and at 1 Re. Furthermore, Krcelic et al. (2020) estimated the fate of ions using the Tsyganenko T96 model and observations of ion velocities observed by Cluster satellites. They suggested that 69 % of the ions escape the magnetosphere, with 50 % in the distant tail. Despite all those interesting studies, the fate of ions observed in the plasma mantle has not yet been well defined. This study aims to clarify whether O$^+$ ion outflows observed in the plasma mantle will escape the magnetosphere and be lost into the solar wind as suggested previously from observations (Slapak et al., 2017; Slapak and Nilsson, 2018; Schillings et al., 2018). For a more accurate estimate of the fate of ions, the starting point should be high altitude, so that much of the transverse heating and centrifugal acceleration are already included. In order to answer this question, we traced particles in a combination of the Tsyganenko T96 (Tsyganenko, 1995) and Weimer 2001 (Weimer, 2001) models. About 25 000 O$^+$ particles were launched from the plasma mantle with initial parameters taken from Cluster observations. This model thus incorporates the effect of the mirror force on the launched ions, centrifugal acceleration, and $E \times B$ drift. It does not include any further wave–particle interaction than what the ions had experienced prior to the observation point.

This paper is organised as follows: Sect. 2 describes the instrumentation and data set we used, followed by the method and a description of our code in Sect. 3. Sections 4 and 5 present and discuss our results respectively. Finally, Sect. 6, summarises our study.

2   Instrument and data

2.1   Cluster and solar wind data

The Cluster mission (Escoubet et al., 2001) consists of four identical spacecraft flying in a tetrahedral formation with an apogee and perigee of approximately 19 and 4 Re respectively. Onboard the spacecraft, the Cluster Ion Spectrometer (CIS) is composed of two instruments: the Hot Ion Analyser (HIA) and the COmposition and DIstribution Function analyser (CODIF) (Rème et al., 2001). The latter provides 3-D distributions of ions with an energy resolution of $\Delta E / E \sim 0.16$, an energy per charge range between 25 and

40 keV q^{-1}, and a 360° field of view. The resolution of the data is usually 4 s; however, it can go up to 16 s. Those features enable observations of O$^+$ in different magnetospheric plasma regions. Additionally, Cluster has a FluxGate Magnetometer (FGM) (Balogh et al., 2001) with a mode sample frequency of 22.4 Hz. In our study, we use the magnetic field averaged over the spacecraft spin period (4 s).

The solar wind data were retrieved from the OMNIWeb database. This database consists of data from several satellites at diverse positions around Earth. In our simulations (see Sect. 3.2), we utilise the solar wind dynamic pressure and velocity, the IMF B_y and B_z components in high resolution (5 min), as well as the magnetic Dst index (1 h).

2.2   Plasma mantle dataset

Our dataset consists of plasma mantle and a few cusp events observed by Cluster spacecraft 4 between 2001 and 2007. In order to only retrieve plasma mantle data, we apply several constraints to the observational data. Firstly, the CODIF O$^+$ counts are contaminated when strong proton fluxes from the magnetosheath are recorded at the same energy level as the O$^+$ ions (Nilsson et al., 2006). These false O$^+$ counts usually originate from the magnetosheath and lead to an underestimate of the O$^+$ velocity moment. The technique to remove these false counts is based on the $E \times B$ drift, because the drift is neither mass nor charge dependent. Consequently, using the kinetic energy equation, the cross-talk signal is seen as an O$^+$ perpendicular bulk velocity that is one-fourth of the corresponding perpendicular proton velocity, and typically the O$^+$ density is higher than 2 cm^{-3} (for more details, we refer the reader to Nilsson et al., 2006). We avoid these contaminated data (and therefore magnetosheath data) using the method described by Nilsson et al. (2006). However, we slightly changed the threshold defined by Nilsson et al. (2006) because over the years the quality of the Cluster data devolved and so did the threshold. The new thresholds are given by $\frac{v_{\text{tot(O}^+)}}{v_{\text{tot(H}^+)}} < 0.2$, $\frac{v_{\text{tot(O}^+)}}{v_{\text{tot(H}^+)}} > 0.5$, or $\frac{N_{\text{O}^+}}{N_{\text{H}^+}} > 0.25$.

To pick out only plasma mantle observations, we implement different conditions for the high-latitude regions. In these regions, the plasma beta β (O$^+$ and H$^+$) is typically higher than 0.05, whereas it is lower than 0.05 in the polar cap (Liao et al., 2010, 2015; Haaland et al., 2017). We use a threshold value of $\beta > 0.1$ for high-latitude regions. Additionally, the perpendicular temperature of the protons should be lower than 1750 eV in order to distinguish plasma sheet from plasma mantle data (Nilsson et al., 2006; Kistler et al., 2006; Slapak et al., 2017). As partly mentioned above, the O$^+$ and H$^+$ densities are restricted to $n(\text{H}^+) > 10^{-3}$ cm^{-3} and 10^{-3} cm$^{-3} < n(\text{O}^+) < 2$ cm^{-3} to keep only reliable velocity estimates. In order to study the fate of ions, we take O$^+$ data with an outward flow ($v_\parallel > 0$ or $v_\parallel < 0$ in the Southern Hemisphere and Northern Hemisphere respectively). Finally, we use a spatial coverage restriction to remove the inner magnetosphere, which is defined by

$-5\,\mathrm{Re} < X_{\mathrm{GSM}} < 8\,\mathrm{Re}$ and $R_{\mathrm{GSM}} = \sqrt{Y_{\mathrm{GSM}}^2 + Z_{\mathrm{GSM}}^2} > 6\,\mathrm{Re}$ (see also Slapak et al., 2017). Major geomagnetic storm data are removed to exclude other magnetospheric regions than the plasma mantle (Schillings et al., 2017). Finally, we also excluded events associated with potential shock arrivals at Earth to avoid strong perturbations in the magnetosphere.

When all the above conditions are met, we define one event by 60 data points or more in a row. Between 2001 and 2007, our automatic routine detected 131 events that met the region criteria and the model restrictions (see Sect. 3.1).

3 Methodology

The section aims at briefly describing how our model works and its inputs and outputs.

3.1 Particle tracing simulations

We use a test particle simulation code (Gunell et al., 2019) to compute ion trajectories in the magnetic fields given by the Tsyganenko T96 model (Tsyganenko, 1995) and electric fields derived from the ionospheric potential given by the Weimer 2001 model (Weimer, 2001). The electric field is defined on a grid, and during the test particle trajectory calculation the electric field at the particle position is found by interpolation. Before the trajectory calculation starts, we define the electrostatic potential V on a three-dimensional grid with a cell size of $1200\,\mathrm{km} \times 1200\,\mathrm{km} \times 1200\,\mathrm{km}$ in the region $-60 < X < 10$, $|Y| < 19$, and $|Z| < 19\,\mathrm{Re}$ by tracing the magnetic field lines from each cell down to the ionosphere, where we retrieve the potential from the Weimer model. The electric field is then found from the relationship $\mathbf{E} = -\nabla V$.

Figure 1 illustrates the magnetic field lines in light grey and the electric field grid in brown. This illustration represents the magnetosphere based on T96 and the grid for the interpolation of the electric field. Due to the limits of the Tsyganenko model, the electric field grid goes to $-60\,\mathrm{Re}$ in the tail and $10\,\mathrm{Re}$ in the dayside (Tsyganenko, 1995). In the north–south, Z, and dawn–dusk, Y, directions, the limit of the grid is at $\pm 19\,\mathrm{Re}$. Note that the illustration is not to scale.

To launch a particle, its initial ion 3-D velocity is calculated using the following equations:

$$v_{\mathbf{tot}} = v_0 + v_{\mathbf{th}},$$
$$v_{\mathbf{tot}} = v_{\parallel}\frac{\boldsymbol{B}}{B} + v_{\boldsymbol{E}\times\boldsymbol{B}} + v_{\mathrm{th}}\frac{\boldsymbol{E}}{E}, \tag{1}$$

where v_0 is the bulk velocity defined by $v_{\parallel}$ and $v_{\boldsymbol{E}\times\boldsymbol{B}}$, the parallel and drift velocities respectively, v_{th} the thermal velocity of the O$^+$ ion (see Sect. 3.2 for more details), B the magnetic field, and E the electric field. Then, the electric field at the position of the O$^+$ ion is formed by interpolation of the field saved on the grid. Finally, from the interpolated
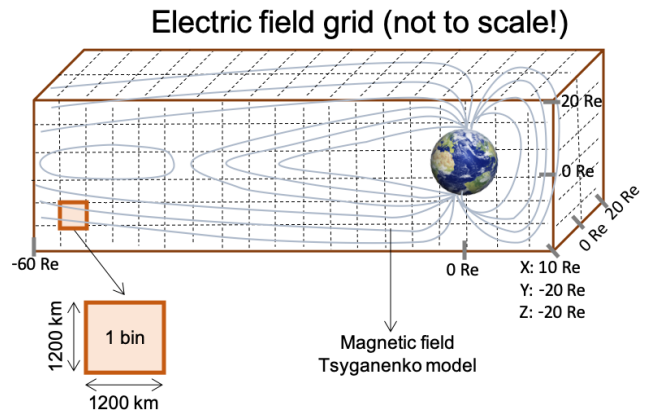
Figure 1. Schematic representation of the modelling of the Earth's environment. The Earth's magnetosphere is represented in light grey and the brown grid displays the electric field grid. Note that the illustration is not to scale.

electric field, a new velocity is calculated with the Boris algorithm (e.g. Birdsall and Langdon, 1991).

The last step is repeated as far as the limitations of the code allow it. The tracing uses a time step based on the gyro-period, so that our time step is $dt = 2\pi/20\omega_c$, whereas the maximum number of iterations is limited to $10\,000$. In $99.93\,\%$ of the cases, the particle stops because they reach the limit of our model (electric field grid), whereas for the $0.07\,\%$ remaining the maximum number of iterations have been completed.

The grid that defined the limit of our model is sufficient for our study because it includes the whole magnetosphere around Earth (magnetopause is defined around $X = 10\,\mathrm{Re}$ in the dayside and about $|Y| = 13$ and $|Z| = 13\,\mathrm{Re}$ for $X = 0\,\mathrm{Re}$). Note that small regions near the subsolar magnetopause are not included; however, they are not relevant for our study. Further in the magnetotail, the magnetopause expands into a "cone shape" in the Y and Z directions and beyond $200\,\mathrm{Re}$ in the X direction. Our grid stops at $X = -60\,\mathrm{Re}$ in the tail due to Tsyganenko model limits; moreover, most of the particles reaching that distance will most likely be lost (see Sects. 4 and 5 for more details). Concerning constraints, the Weimer model imposes no constraints on solar wind parameters, while Tsyganenko T96 does. Therefore, when an observation meets the criteria described above, it also has to match with Tsyganenko T96 constraints, which concerns the Dst index ($-100\,\mathrm{nT} < \mathrm{Dst} < 20\,\mathrm{nT}$), the dynamic pressure ($0.5\,\mathrm{nPa} < P_{\mathrm{dyn}} < 10\,\mathrm{nPa}$), and IMF B_z and B_y ($-10\,\mathrm{nT} < B_z, B_y < 10\,\mathrm{nT}$).

3.2 Inputs and outputs of the model

The inputs of the models are (a) solar wind parameters as required by the Tsyganenko and Weimer models and (b) the positions and thermal and bulk parallel velocities, $v_{\parallel}$ and v_{th} respectively, based on Cluster observations. The solar wind
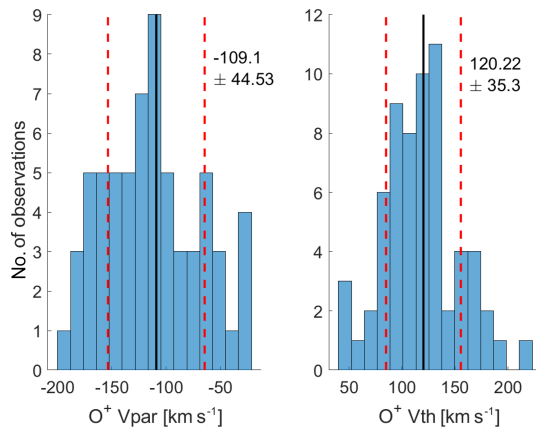
Figure 2. Cluster SC4 observations: parallel and thermal components of the O$^+$ velocity on 11 June 2001 between 01:24 and 01:29 UT. The solid black line represents the mean and the dashed red lines show the standard deviations.

parameters (see Sect. 2.1) are taken at the initial time of each corresponding event. The 131 plasma mantle events are automatically detected by a routine scanning Cluster datum (see Sect. 2.2). During these events, we calculate the thermal and bulk parallel velocities and retrieve the spacecraft positions. These parameters are then used to create the initial positions and $v_\parallel$ and v_{th} of 200 O$^+$ ions (per event) that we trace forward in time.

Figure 2 shows the bulk parallel and thermal velocities from Cluster data from a sample event in the Northern Hemisphere. This plasma mantle event occurred on 11 June 2001 between 01:24 and 01:29 UT. The solid black line shows the weighted mean defined by $\sum v_{\parallel,i} n_i / \sum n_i$ (where i denotes the observations, typically one 4 s measurement for CODIF), whereas the dashed red lines display the standard deviations. For this event, the mean $v_\parallel(O^+)$ is -109.01 ± 44.54 km s^{-1} and the $v_{th}(O^+)$ is 120.22 ± 35.3 km s^{-1}. A uniform standard distribution of random values in these intervals $v_\parallel = [-64.47; -153.55]$ km s^{-1} and $v_{th} = [84.92; 155.52]$ km s^{-1} gives the initial $v_\parallel$ and v_{th} utilised as inputs for the forward traced particles. In a similar way, the initial positions of the 200 traced O$^+$ particles are randomly chosen in the interval $x = [2.046; 2.061]$, $y = [-8.643; -8.558]$, $z = [8.885; 8.886]$, which are the minimum and maximum positions of Cluster during the event (11 June 2001 – approximately 5 min).

The output of the model gives us the final positions of O$^+$ in the magnetosphere as well as the travelling times of the particles in the magnetosphere.

4 Observations and results

We analysed 131 events based on Cluster observations between 2001 and 2007. For each event, we launched 200 O$^+$ ions with various perpendicular and parallel velocities.

Therefore, the statistics presented in this section are based on 26 200 O$^+$ ions starting in the high-altitude regions. Their ending positions are spread within the magnetosphere, but a significant number end up at the limit of our model. Figure 3 shows an example of 40 O$^+$ trajectories (out of the 200 computed) spread in the magnetosphere. This event occurred on 11 June 2001 during approximately 5 min (01:24–01:29 UT); the Dst index was -10 nT with a slightly southward IMF ($B_z = -0.486$ nT) and negative By (-1.16 nT). The solar wind velocity was around 550 km s^{-1} and the dynamic pressure 1.74 nPa. The top panel in Fig. 3 displays the trajectories in the XZ plane, while the middle and bottom panels display the YZ and XY planes respectively. The different colours represent various trajectories, the crosses show the initial positions (denoted by starting positions), whereas the asterisks show the final positions. This event clearly shows that ions from similar positions but with different velocities (see Fig. 2 for the velocity range) can have very distinct trajectories. Part of the O$^+$ ions follow the magnetic field lines and stop at -60 Re in the distant tail (limit of the model); others mirror a few times before being lost on the flank (see bottom panel). Finally, a few ions mirror back and forth around Earth and end up in the cusp, in the polar cap, or simply in the plasma sheet. In this event (Fig. 3), 191 trajectories out of the 200 computed are considered to be long (more than 2000 iteration steps; see the next paragraph for more details). In other events, we observed ions following magnetic field lines into the distant tail that eventually reach the plasma sheet around $X = -50$ Re and turn back toward Earth (not shown). Those particles are return flow (earthward flow), and we discuss their fate in the Discussion (see Sect. 5).

Figure 3 provides a good example of how differently the trajectories could be spread starting from a similar position; however, this particular example is not representative of our sample events. Since the plasma mantle is close to the magnetopause, some events (17 %) have very short trajectories (approximately 5 min). Indeed, the O$^+$ ions that are launched at high altitudes in the plasma mantle typically follow the magnetic field lines and reach the magnetopause almost immediately. Those ions escape into the magnetosheath and will most likely never turn back to the magnetosphere.

We analysed the fate of the ions with short (lower than 200 steps, average time 5 min), middle (200 to 2000 steps, average time 20 min), and long (over 2000 steps, average time 104 min) trajectories. Similarly to Fig. 3, Fig. 4 shows a sample of 25 trajectories in the XZ and XY planes of each division, whereas the length of the 26 200 trajectories in our sample is shown in Fig. 5a. The mean trajectory is about 767 iteration steps (or $10^{2.65}$ in the panel). We found that O$^+$ trajectories with less than 2000 steps (short and middle) escape mainly from the flank of the magnetosphere and represent 95 % of our samples. Ions with longer trajectories represent 5 % of the total sample. Within the ions with a long trajectory, 35.5 % end up in the near-Earth plasma sheet (at geocentric distance lower than 10 Re). We defined

11/06/2001 01:24 – 01:29 UT
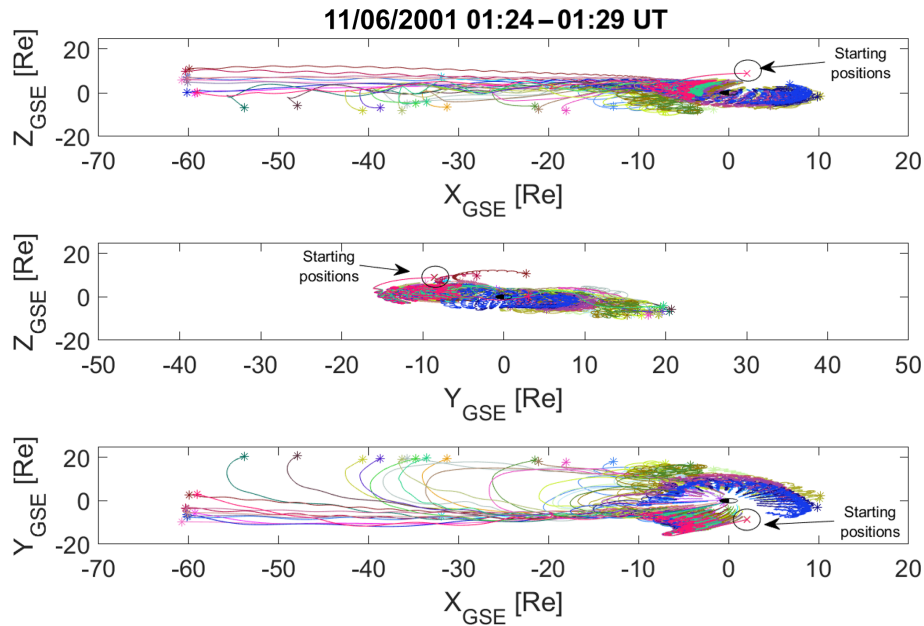
Figure 3. Example of 40 O$^+$ varied trajectories (different colours) from the plasma mantle on 11 June 2001 between 01:24 and 01:29 UT. The crosses denote the starting positions, whereas the asterisks denote the ending positions in the magnetosphere.

the escaping limit by the geocentric distance of the final positions $R = \sqrt{X_{\mathrm{fin}}^2 + Y_{\mathrm{fin}}^2 + Z_{\mathrm{fin}}^2}$ that equals 10 Re (see Fig. 5b). Thus, an ion is defined as having escaped the magnetosphere if its final position is outside 10 Re. This is justified by the fact that if the tracing does not end due to the limits of iterations, such ions have left the simulation domain (except for 0.07 % of the trajectories; see Sect. 3.1). Note that the minimum geocentric distance where the O$^+$ ions are launched is 7.64 Re (not shown). Only 2 % of the total trajectories have their final positions below this limit (10 Re); hence, 98 % of the ions are escaping the magnetosphere. The geocentric distance R of the 26 200 final positions is represented in the middle panel (b) of Fig. 5. The O$^+$ average final position is $R = 22.9$ Re.

Furthermore, in Fig. 5c, we determined the minimum distance in the X direction for each trajectory as the minimum value found in the X direction of each ion trajectory (given in Re). As an example, for a trajectory of 2000 steps, the minimum X distance is the minimum value (in the X direction) within the 2000 steps, which is not necessarily the final position of the ion. In Fig. 5c, each data point represents the minimum X distance of one trajectory. The average minimum X distance is around −10 Re, which corresponds to the plasma mantle region if $|Z| > 5$ Re (see also in Fig. 6). This parameter is important because some particles that interact with the plasma sheet in the distant tail might come back close to Earth. However, such cases are rare because for a total of 849 trajectories with an X minimum distance beyond −50 Re, only 23 trajectories finish their route close to Earth

($R < 10$ Re). The 826 remaining are roughly equally spread between 10 and 64 Re.

Figure 6 shows the start (panels a–c) and stop (panels d–f) positions of the O$^+$ trajectories in cylindrical coordinates ($R_{\mathrm{cyl}} = \sqrt{Y^2 + Z^2}$). The columns give the length of the trajectories: short, middle, and long as defined above. The colour bar represents the number of trajectories per bin (1 Re × 1 Re) and the red dashed line represents the average magnetopause for the corresponding events. In the first line, we clearly see that particles are launched in the plasma mantle region, while in the second one, the ending positions are spread at high R_{cyl}. O$^+$ ions from the plasma mantle do not necessarily escape in the distant tail as we suggested in Slapak et al. (2017) and Schillings et al. (2019), but they do escape almost directly through the magnetopause because of their high velocities in these regions. The magnetopause is identified by abrupt changes in the tracing of the magnetic field lines; once the magnetopause is crossed, the field lines become straight and follow the IMF direction. Similarly, we observe 22 % of the ions escaping in the dayside ($X > 0$ Re). Note that the vertical line of ions at −60 Re represents ions whose tracing has been stopped due to the limit of our code.

The associated scaled O$^+$ flux (defined as the net outward flux mapped to an ionospheric reference altitude of 1000 km with a magnetic strength of 50 000 nT) is about 10^{13} m^{-2} s^{-1} on average (not shown). The highest O$^+$ scaled flux, 10^{14} m^{-2} s^{-1}, is observed around Earth (−3 Re < X < 3 Re) at $R_{\mathrm{cyl}} = 23$ Re. In contrast, the lower scaled flux is observed below $R_{\mathrm{cyl}} = 10$ Re and between 15 Re < R_{cyl} < 20 Re for X lower than −20 Re.
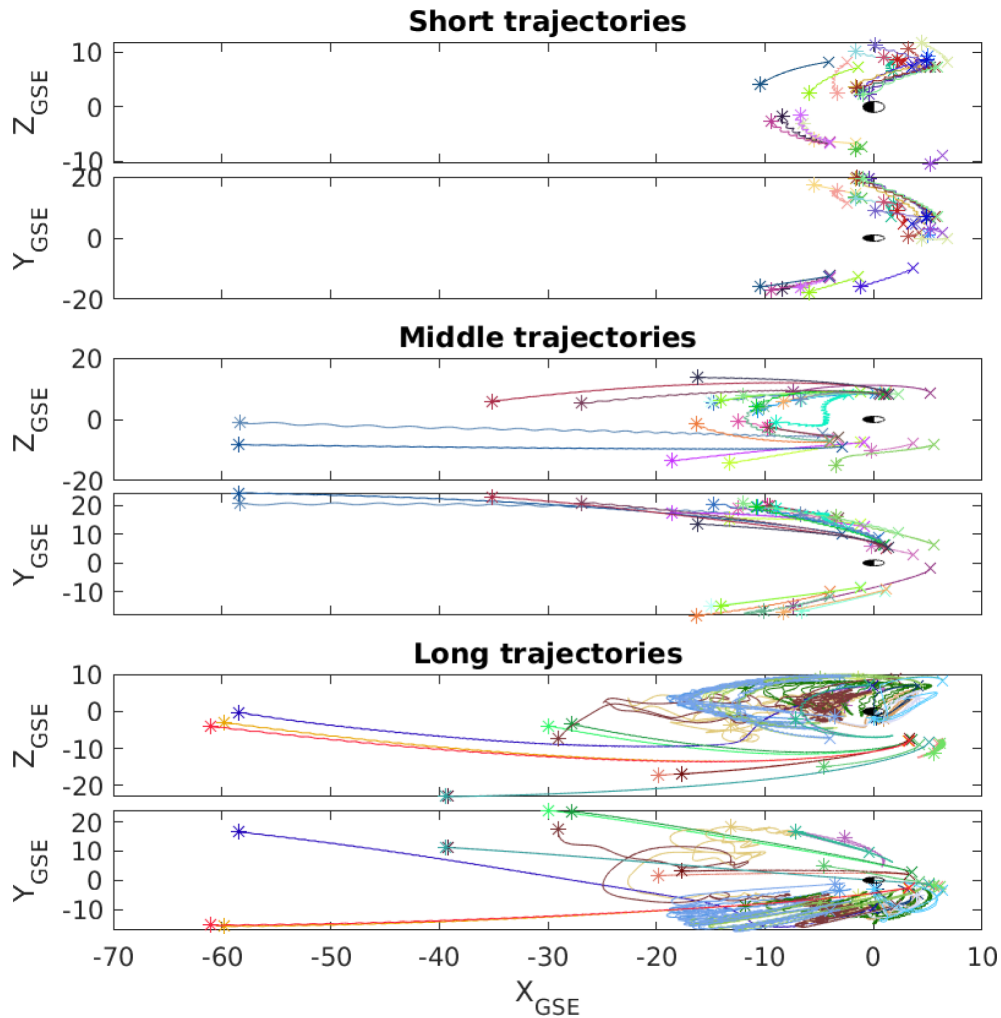
Figure 4. Sample of 25 short, middle, and long trajectories in the XZ and XY planes. Units of the axes are in Re. Each colour represents one trajectory, and the crosses and the asterisks show the initial and final position respectively.
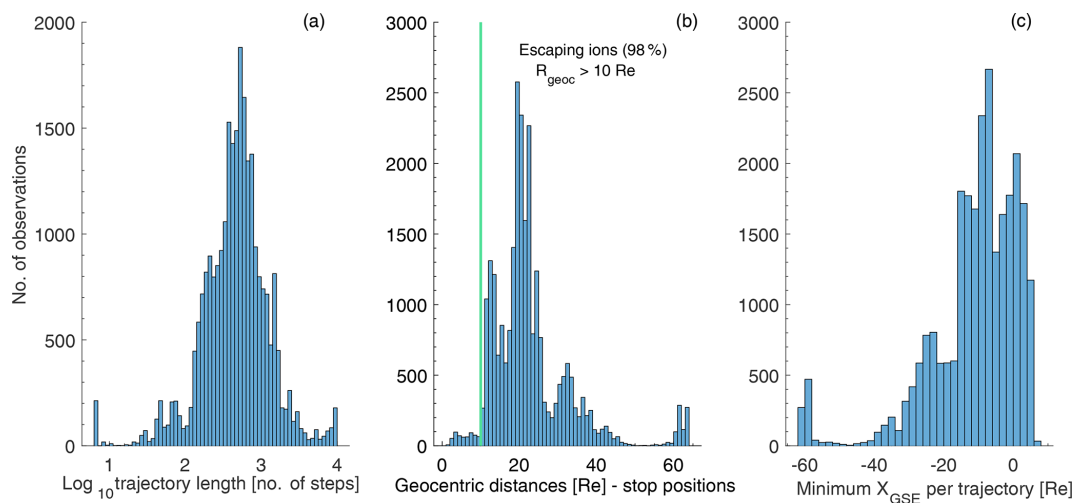
Figure 5. (a) Length of the 26 200 O$^+$ trajectories in our sample. Note the logarithmic scale. **(b)** Final positions expressed in the geocentric distance R given in Re (see text for definition). **(c)** Minimum X distance for each trajectory.
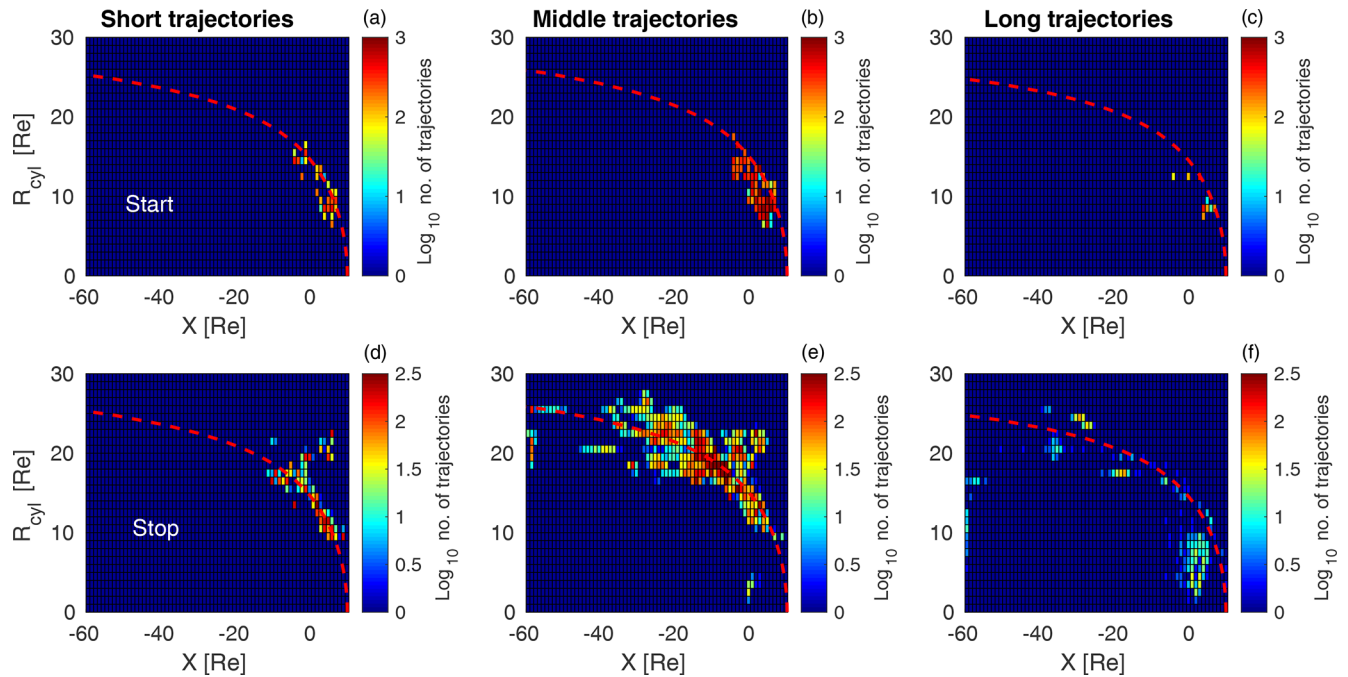
Figure 6. Cylindrical coordinates of the starting and ending positions of the launched O^+ ions depending on the length of their trajectory (see definitions in the text). Panels **a–c** show the starting positions, while the panels **d–f** show the ending positions. The colour bar represents the number of trajectories in each bin. The red dashed line shows the average magnetopause for the corresponding events.

5 Discussion

In our 131 events based on Cluster-CODIF observations, the parallel and thermal components of the velocities during the events are taken as inputs to our forward tracing model (see Sect. 3.2 and Fig. 2). From these observations, we found that O^+ ions observed in the plasma mantle have a parallel velocity comparable to or lower than the thermal velocity, as expected. More precisely, the ratio between the velocity components ($|v_\parallel|/v_{\mathrm{th}}$) is 0.65 ± 0.44. Since the bulk perpendicular velocity is much smaller than the parallel bulk velocity in the plasma mantle (Vaith et al., 2004), the O^+ ions in the mantle can be characterised by the parallel bulk velocity and the thermal velocity. The bulk perpendicular velocity is relatively small but would be important for their trajectories, in particular, storm time and/or southward IMF (Haaland et al., 2008). Indeed, in the 13 % of our events with higher convection velocity, more than half have a corresponding Dst index below -20 nT and a southward IMF.

We do not find any strong correlation between geomagnetic activity (Dst) and the final positions (see Fig. 7). For the IMF direction, we identify 48 % of the events as being associated with northward IMF (see the right-hand side of the vertical dashed line in Fig. 7) and the final positions of these ions as being mainly spread between $R = 10$ and $R = 40$ Re (95 % of the events with northward IMF). On the left-hand side of the vertical dashed line in Fig. 7, a similar trend is observed for the remaining 52 % of events associated
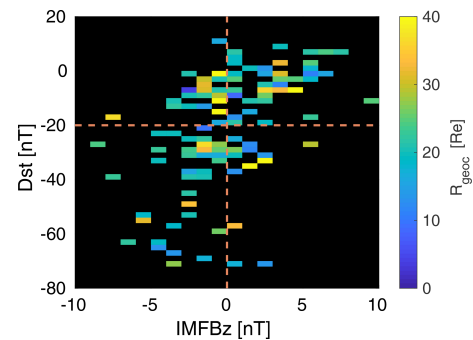
Figure 7. Geocentric final positions of all O^+ ions (colour bar) as a function of geomagnetic activity (Dst) and IMF B_z direction. The horizontal and vertical dashed lines divide quiet (top) from disturbed (bottom) geomagnetic activity and southward (left) from northward (right) IMF respectively.

with southward IMF. Thus, the direction of the IMF does not significantly affect the final location of the ions. However, if we consider only the ions with their ending positions in $R < 10$ Re, they occur during southward IMF (67 %). This result can be compared to the cold ion outflow observed in the lobes during southward IMF. Haaland et al. (2012) found that for southward IMF the cold ion outflow is convected toward the plasma sheet due to strong convection, whereas for the IMF directed northward convection is stagnant, so that cold ion outflow reaches the far tail.

Slapak et al. (2012) suggested three main routes for ion outflow: (1) cold ions that will end up mainly in the plasma sheet (Mouikis et al., 2010; Haaland et al., 2012; Liao et al., 2015), (2) energised ions from the cusp to the plasma mantle (Liao et al., 2010; Slapak et al., 2017; Schillings et al., 2019), and (3) energised ions from the cusp going directly to the magnetosheath (Slapak et al., 2017). Slapak et al. (2017), Slapak and Nilsson (2018), and Schillings et al. (2019) suggested that ions observed in the plasma mantle have sufficient energy and velocity to escape in the distant tail. However, our results show that very few ions reach the distant tail, but instead escape directly through the magnetopause after a few minutes (~ 17 min). These O^+ ions have short or middle length trajectories in our model (less than 2000 steps; see also Sect. 4) and represent 95 % of our sample. Most (99.6 %) of these O^+ ions reach a point where the tracing is stopped at a geocentric distance higher than 10 Re and escape the magnetosphere. For ions with trajectories longer than 2000 steps (5 % of the total trajectories), 35 % is earthward flow due to its interaction with the plasma sheet. Most of these ions do not return to the ionosphere. Some will instead experience charge exchange, become neutral, and be lost from the magnetosphere. This assumption is supported by Ebihara et al. (2006), who modelled O^+ trajectories and introduce a charge exchange process in their model. They estimated that 2 % of the total outflow became neutral due to charge exchange with the hydrogen geocorona. Other particles will drift to the magnetopause (magnetopause shadowing) and be lost. We note that ion precipitation recorded by the DMSP spacecraft (Newell et al., 2007) indicates a total precipitation of ions (H^+ and O^+) of the order 10^{24} s^{-1}, which is most of the time dominated by cusp precipitation, not return flow precipitation. This is even less than the return flow estimated by Slapak and Nilsson (2018), indicating that most return flow indeed does not precipitate to the ionosphere. However, we do not study the fate of this earthward ion flow, and therefore they are not considered to be escaping ions in this study.

Under quiet magnetospheric conditions (Dst ≥ -20 nT; see Fig. 7, horizontal dashed line), it was found that 3 % of the final positions of the trajectories are within a geocentric distance of 10 Re (return flow), whereas during disturbed conditions we observe only 1.6 % return flow. This result agrees with Ebihara et al. (2006), who found that under quiet time 4 % to 7 % of the outflowing ions return to Earth. Under disturbed conditions, the authors estimated a smaller return of 0.6 % to 0.8 %.

Finally, since O^+ ions are launched from the plasma mantle, the particles observed by CODIF already went through transverse heating and centrifugal acceleration. Thus, this model includes most of the energisation and acceleration compared to other models. Moreover, the model does not include wave–particle interaction after the oxygen ion has been launched.

6 Summary and conclusions

Based on previous suggestions that O^+ ions from the plasma mantle are escaping (Slapak et al., 2017; Slapak and Nilsson, 2018; Schillings et al., 2019), we investigate the fate of ions by tracing the particles forward in time in the magnetosphere. The magnetosphere is represented by the Tsyganenko T96 model for the magnetic field and the Weimer 2001 model for the electric field (ionospheric potential). We analyse 131 plasma mantle events detected automatically in the Cluster data during 2001 and 2007. For each event, 200 O^+ ions with an initial parallel and perpendicular velocity are launched from the plasma mantle. The initial velocities and positions are determined by Cluster observations and are used as inputs for the forward tracing. Our results are summarised in the following points.

1. The O^+ ions observed in the plasma mantle have an initial parallel velocity lower than the thermal velocity, as expected. Thus, the thermal velocity dominates from the start, and through high perpendicular temperatures, the mirror force will increase the parallel velocity further downstream of the observation point.

2. 98 % of the final positions (out of 26 200) are located beyond a geocentric distance of 10 Re. These particles escape and are lost into the solar wind; 20 % of the ions escape directly through the high-latitude dayside magnetopause.

3. 2 % of the total trajectories lead back towards earth; i.e. they constitute return flow. Some of these O^+ ions have interacted with the plasma sheet in the distant tail and eventually end up between the Earth and a geocentric distance of 10 Re.

4. Under disturbed magnetospheric conditions (Dst < -20 nT), we observe 1.6 % return flow, whereas during quiet time the return flow increases to 3 %.

5. We do not find any correlation between the IMF direction, the geomagnetic disturbances, and the final positions of O^+ in our tracing model. However, the ions ending up close to the Earth (geocentric distance smaller than 10 Re) are for 67 % of the time associated with southward IMF.

References

Abe, T., Whalen, B. A., Yau, A. W., Horita, R. E., Watanabe, S., and Sagawa, E.: EXOS D (Akebono) suprathermal mass spectrometer observations of the polar wind, J. Geophys. Res.-Space, 98, 11191–11203, https://doi.org/10.1029/92JA01971, 1993.

Abudayyeh, H. A., Barghouthi, I. A., Slapak, R., and Nilsson, H.: Centrifugal acceleration at high altitudes above the polar cap: A Monte Carlo simulation, J. Geophys. Res.-Space, 120, 6409–6426, https://doi.org/10.1002/2015JA021325, 2015.

André, M. and Cully, C. M.: Low-energy ions: A previously hidden solar system particle population, Geophys. Res. Lett., 39, L03101, https://doi.org/10.1029/2011GL050242, 2012.

Arvelius, S., Yamauchi, M., Nilsson, H., Lundin, R., Hobara, Y., Rème, H., Bavassano-Cattaneo, M. B., Paschmann, G., Korth, A., Kistler, L. M., and Parks, G. K.: Statistics of high-altitude and high-latitude O$^+$ ion outflows observed by Cluster/CIS, Ann. Geophys., 23, 1909–1916, https://doi.org/10.5194/angeo-23-1909-2005, 2005.

Axford, W. I.: The polar wind and the terrestrial helium budget, J. Geophys. Res., 73, 6855–6859, https://doi.org/10.1029/JA073i021p06855, 1968.

Balogh, A., Carr, C. M., Acuña, M. H., Dunlop, M. W., Beek, T. J., Brown, P., Fornaçon, K.-H., Georgescu, E., Glassmeier, K.-H., Harris, J., Musmann, G., Oddy, T., and Schwingenschuh, K.: The Cluster Magnetic Field Investigation: overview of in-flight performance and initial results, Ann. Geophys., 19, 1207–1217, https://doi.org/10.5194/angeo-19-1207-2001, 2001.

Barakat, A. R. and Schunk, R. W.: A three-dimensional model of the generalized polar wind, J. Geophys. Res.-Space, 111, A12314, https://doi.org/10.1029/2006JA011662, 2006.

Barghouthi, I. A., Abudayyeh, H. A., Slapak, R., and Nilsson, H.: O$^+$ and H$^+$ above the polar cap: Observations and semikinetic simulations, J. Geophys. Res.-Space, 121, 459–474, https://doi.org/10.1002/2015JA021990, 2016.

Birdsall, C. K. and Langdon, A.: Plasma Physics via Computer Simulation, IOP Publishing Ltd Techno House, Bristol, England, New York, NY, USA, ISBN 0 7503 1025 1, 1991.

Chappell, C. R., Moore, T. E., and Waite Jr., J. H.: The ionosphere as a fully adequate source of plasma for the earth's magnetosphere, J. Geophys. Res., 92, 5896–5910, https://doi.org/10.1029/JA092iA06p05896, 1987.

Cluster Science Archive: Welcome to the cluster science archive, available at: https://csa.esac.esa.int/csa-web/, last access: June 2020.

Ebihara, Y., Yamada, M., Watanabe, S., and Ejiri, M.: Fate of outflowing suprathermal oxygen ions that originate in the polar ionosphere, J. Geophys. Res.-Space, 111, A04219, https://doi.org/10.1029/2005JA011403, 2006.

Engwall, E., Eriksson, A. I., Cully, C. M., André, M., Puhl-Quinn, P. A., Vaith, H., and Torbert, R.: Survey of cold ionospheric outflows in the magnetotail, Ann. Geophys., 27, 3185–3201, https://doi.org/10.5194/angeo-27-3185-2009, 2009.

Escoubet, C. P., Fehringer, M., and Goldstein, M.: Introduction: The Cluster mission, Ann. Geophys., 19, 1197–1200, https://doi.org/10.5194/angeo-19-1197-2001, 2001.

Gunell, H., Maggiolo, R., Nilsson, H., Stenberg Wieser, G., Slapak, R., Lindkvist, J., Hamrin, M., and De Keyser, J.: Why an intrinsic magnetic field does not protect a planet against atmospheric escape, Astron. Astrophys., 614, L3, https://doi.org/10.1051/0004-6361/201832934, 2018.

Gunell, H., De Spiegeleer, A., and Schillings, A.: ham – a particle tracing code for Earth's magnetosphere, https://doi.org/10.5281/zenodo.3466771, 2019.

Haaland, S., Paschmann, G., Förster, M., Quinn, J., Torbert, R., Vaith, H., Puhl-Quinn, P., and Kletzing, C.: Plasma convection in the magnetotail lobes: statistical results from Cluster EDI measurements, Ann. Geophys., 26, 2371–2382, https://doi.org/10.5194/angeo-26-2371-2008, 2008.

Haaland, S., Lybekk, B., Svenes, K., Pedersen, A., Förster, M., Vaith, H., and Torbert, R.: Plasma transport in

the magnetotail lobes, Ann. Geophys., 27, 3577–3590, https://doi.org/10.5194/angeo-27-3577-2009, 2009.

Haaland, S., Eriksson, A., Engwall, E., Lybekk, B., Nilsson, H., Pedersen, A., Svenes, K., André, M., Förster, M., Li, K., Johnsen, C., and Østgaard, N.: Estimating the capture and loss of cold plasma from ionospheric outflow, J. Geophys. Res.-Space, 117, A07311, https://doi.org/10.1029/2012JA017679, 2012.

Haaland, S., Lybekk, B., Maes, L., Laundal, K., Pedersen, A., Tenfjord, P., Ohma, A., Østgaard, N., Reistad, J., and Snekvik, K.: North–south asymmetries in cold plasma density in the magnetotail lobes: Cluster observations, J. Geophys. Res.-Space, 122, 136–149, https://doi.org/10.1002/2016JA023404, 2017.

Hoffman, J. H.: Ion composition measurements in the polar region from the Explorer 31 satellite, Trans. Am. Geophys. Union, 49, 253, 1968.

Horwitz, J. L., Ho, C. W., Scarbro, H. D., Wilson, G. R., and Moore, T. E.: Centrifugal acceleration of the polar wind, J. Geophys. Res.-Space, 99, 15051–15064, https://doi.org/10.1029/94JA00924, 1994.

Kistler, L. M. and Mouikis, C. G.: The inner magnetosphere ion composition and local time distribution over a solar cycle, J. Geophys. Res.-Space, 121, 2009–2032, https://doi.org/10.1002/2015JA021883, 2016.

Kistler, L. M., Mouikis, C. G., Cao, X., Frey, H., Klecker, B., Dandouras, I., Korth, A., Marcucci, M. F., Lundin, R., McCarthy, M., Friedel, R., and Lucek, E.: Ion composition and pressure changes in storm time and nonstorm substorms in the vicinity of the near-Earth neutral line, J. Geophys. Res.-Space, 111, A11222, https://doi.org/10.1029/2006JA011939, 2006.

Krcelic, P., Haaland, S., Maes, L., Slapak, R., and Schillings, A.: Estimating the fate of oxygen ion outflow from the high-altitude cusp, Ann. Geophys., 38, 491–505, https://doi.org/10.5194/angeo-38-491-2020, 2020.

Li, K., Haaland, S., Eriksson, A., André, M., Engwall, E., Wei, Y., Kronberg, E. A., Fränz, M., Daly, P. W., Zhao, H., and Ren, Q. Y.: On the ionospheric source region of cold ion outflow, Geophys. Res. Lett., 39, L18102, https://doi.org/10.1029/2012GL053297, 2012.

Liao, J., Kistler, L. M., Mouikis, C. G., Klecker, B., Dandouras, I., and Zhang, J.-C.: Statistical study of O$^+$ transport from the cusp to the lobes with Cluster CODIF data, J. Geophys. Res.-Space, 115, A00J15, https://doi.org/10.1029/2010JA015613, 2010.

Liao, J., Kistler, L. M., Mouikis, C. G., Klecker, B., and Dandouras, I.: Acceleration of O$^+$ from the cusp to the plasma sheet, J. Geophys. Res.-Space, 120, 1022–1034, https://doi.org/10.1002/2014JA020341, 2015.

Mouikis, C. G., Kistler, L. M., Liu, Y. H., Klecker, B., Korth, A., and Dandouras, I.: H$^+$ and O$^+$ content of the plasma sheet at 15–19 Re as a function of geomagnetic and solar activity, J. Geophys. Res.-Space, 115, A00J16, https://doi.org/10.1029/2010JA015978, 2010.

NASA Goddard Space Flight Center: OMNIWeb Plus, available at: https://omniweb.gsfc.nasa.gov/, last access: June 2020.

Newell, P. T., Sotirelis, T., Liou, K., Meng, C.-I., and Rich, F. J.: A nearly universal solar wind-magnetosphere coupling function inferred from 10 magnetospheric state variables, J. Geophys. Res.-Space, 112, A01206, https://doi.org/10.1029/2006JA012015, 2007.

Nilsson, H.: Heavy Ion Energization, Transport, and Loss in the Earth's Magnetosphere, in: The Dynamic Magnetosphere, edited by: Liu, W. and Fujimoto, M., Springer Netherlands, Dordrecht, 315–327, https://doi.org/10.1007/978-94-007-0501-2_17, 2011.

Nilsson, H., Waara, M., Arvelius, S., Marghitu, O., Bouhram, M., Hobara, Y., Yamauchi, M., Lundin, R., Rème, H., Sauvaud, J.-A., Dandouras, I., Balogh, A., Kistler, L. M., Klecker, B., Carlson, C. W., Bavassano-Cattaneo, M. B., and Korth, A.: Characteristics of high altitude oxygen ion energization and outflow as observed by Cluster: a statistical study, Ann. Geophys., 24, 1099–1112, https://doi.org/10.5194/angeo-24-1099-2006, 2006.

Nilsson, H., Waara, M., Marghitu, O., Yamauchi, M., Lundin, R., Rème, H., Sauvaud, J.-A., Dandouras, I., Lucek, E., Kistler, L. M., Klecker, B., Carlson, C. W., Bavassano-Cattaneo, M. B., and Korth, A.: An assessment of the role of the centrifugal acceleration mechanism in high altitude polar cap oxygen ion outflow, Ann. Geophys., 26, 145–157, https://doi.org/10.5194/angeo-26-145-2008, 2008.

Nilsson, H., Barghouthi, I. A., Slapak, R., Eriksson, A. I., and André, M.: Hot and cold ion outflow: Spatial distribution of ion heating, J. Geophys. Res.-Space, 117, A11201, https://doi.org/10.1029/2012JA017974, 2012.

Norqvist, P., André, M., and Tyrland, M.: A statistical study of ion energization mechanisms in the auroral region, J. Geophys. Res.-Space, 103, 23459–23473, https://doi.org/10.1029/98JA02076, 1998.

Peterson, W. K., Collin, H. L., Yau, A. W., and Lennartsson, O. W.: Polar/Toroidal Imaging Mass – Angle Spectrograph observations of suprathermal ion outflow during solar minimum conditions, J. Geophys. Res.-Space, 106, 6059–6066, https://doi.org/10.1029/2000JA003006, 2001.

Rème, H., Aoustin, C., Bosqued, J. M., Dandouras, I., Lavraud, B., Sauvaud, J. A., Barthe, A., Bouyssou, J., Camus, T., Coeur-Joly, O., Cros, A., Cuvilo, J., Ducay, F., Garbarowitz, Y., Medale, J. L., Penou, E., Perrier, H., Romefort, D., Rouzaud, J., Vallat, C., Alcaydé, D., Jacquey, C., Mazelle, C., D'Uston, C., Möbius, E., Kistler, L. M., Crocker, K., Granoff, M., Mouikis, C., Popecki, M., Vosbury, M., Klecker, B., Hovestadt, D., Kucharek, H., Kuenneth, E., Paschmann, G., Scholer, M., Sckopke, N., Seidenschwang, E., Carlson, C. W., Curtis, D. W., Ingraham, C., Lin, R. P., McFadden, J. P., Parks, G. K., Phan, T., Formisano, V., Amata, E., Bavassano-Cattaneo, M. B., Baldetti, P., Bruno, R., Chionchio, G., di Lellis, A., Marcucci, M. F., Pallocchia, G., Korth, A., Daly, P. W., Graeve, B., Rosenbauer, H., Vasyliunas, V., McCarthy, M., Wilber, M., Eliasson, L., Lundin, R., Olsen, S., Shelley, E. G., Fuselier, S., Ghielmetti, A. G., Lennartsson, W., Escoubet, C. P., Balsiger, H., Friedel, R., Cao, J.-B., Kovrazhkin, R. A., Papamastorakis, I., Pellat, R., Scudder, J., and Sonnerup, B.: First multispacecraft ion measurements in and near the Earth's magnetosphere with the identical Cluster ion spectrometry (CIS) experiment, Ann. Geophys., 19, 1303–1354, https://doi.org/10.5194/angeo-19-1303-2001, 2001.

Rosenbauer, H., Grünwaldt, H., Montgomery, M. D., Paschmann, G., and Sckopke, N.: Heos 2 plasma observations in the distant polar magnetosphere: The plasma mantle, J. Geophys. Res., 80, 2723–2737, https://doi.org/10.1029/JA080i019p02723, 1975.

Schillings, A., Nilsson, H., Slapak, R., Yamauchi, M., and Westerberg, L.-G.: Relative outflow enhancements during major ge-

omagnetic storms – Cluster observations, Ann. Geophys., 35, 1341–1352, https://doi.org/10.5194/angeo-35-1341-2017, 2017.

Schillings, A., Nilsson, H., Slapak, R., Wintoft, P., Yamauchi, M., Wik, M., Dandouras, I., and Carr, C. M.: O^+ Escape During the Extreme Space Weather Event of 4–10 September 2017, Space Weather, 16, 1363–1376, https://doi.org/10.1029/2018SW001881, 2018.

Schillings, A., Slapak, R., Nilsson, H., Yamauchi, M., Dandouras, I., and Westerberg, L.-G.: Earth atmospheric loss through the plasma mantle and its dependence on solar wind parameters, Earth Planets Space, 71, 70, https://doi.org/10.1186/s40623-019-1048-0, 2019.

Schunk, R. W. and Sojka, J. J.: A three-dimensional time-dependent model of the polar wind, J. Geophys. Res.-Space, 94, 8973–8991, https://doi.org/10.1029/JA094iA07p08973, 1989.

Schunk, R. W. and Sojka, J. J.: Global ionosphere-polar wind system during changing magnetic activity, J. Geophys. Res.-Space, 102, 11625–11651, https://doi.org/10.1029/97JA00292, 1997.

Sharp, R. D., Johnson, R. G., and Shelley, E. G.: Observation of an ionospheric acceleration mechanism producing energetic (keV) ions primarily normal to the geomagnetic field direction, J. Geophys. Res., 82, 3324–3328, https://doi.org/10.1029/JA082i022p03324, 1977.

Shelley, E. G., Sharp, R. D., and Johnson, R. G.: Satellite observations of an ionospheric acceleration mechanism, Geophys. Res. Lett., 3, 654–656, https://doi.org/10.1029/GL003i011p00654, 1976.

Slapak, R. and Nilsson, H.: The Oxygen Ion Circulation in The Outer Terrestrial Magnetosphere and Its Dependence on Geomagnetic Activity, Geophys Res. Lett., 45, 12669–12676, https://doi.org/10.1029/2018GL079816, 2018.

Slapak, R., Nilsson, H., Waara, M., André, M., Stenberg, G., and Barghouthi, I. A.: O^+ heating associated with strong wave activity in the high altitude cusp and mantle, Ann. Geophys., 29, 931–944, https://doi.org/10.5194/angeo-29-931-2011, 2011.

Slapak, R., Nilsson, H., Westerberg, L. G., and Eriksson, A.: Observations of oxygen ions in the dayside magnetosheath associated with southward IMF, J. Geophys. Res.-Space, 117, A07218, https://doi.org/10.1029/2012JA017754, 2012.

Slapak, R., Schillings, A., Nilsson, H., Yamauchi, M., Westerberg, L.-G., and Dandouras, I.: Atmospheric loss from the dayside open polar region and its dependence on geomagnetic activity: implications for atmospheric escape on evolutionary timescales, Ann. Geophys., 35, 721–731, https://doi.org/10.5194/angeo-35-721-2017, 2017.

Strangeway, R. J., Ergun, R. E., Su, Y., Carlson, C. W., and Elphic, R. C.: Factors controlling ionospheric outflows as observed at intermediate altitudes, J. Geophys. Res.-Space, 110, A03221, https://doi.org/10.1029/2004JA010829, 2005.

Tsyganenko, N. A.: Modeling the Earth's magnetospheric magnetic field confined within a realistic magnetopause, J. Geophys. Res.-Space, 100, 5599–5612, https://doi.org/10.1029/94JA03193, 1995.

Vaith, H., Paschmann, G., Quinn, J. M., Förster, M., Georgescu, E., Haaland, S. E., Klecker, B., Kletzing, C. A., Puhl-Quinn, P. A., Rème, H., and Torbert, R. B.: Plasma convection across the polar cap, plasma mantle and cusp: Cluster EDI observations, Ann. Geophys., 22, 2451–2461, https://doi.org/10.5194/angeo-22-2451-2004, 2004.

Waara, M., Slapak, R., Nilsson, H., Stenberg, G., André, M., and Barghouthi, I. A.: Statistical evidence for O^+ energization and outflow caused by wave-particle interaction in the high altitude cusp and mantle, Ann. Geophys., 29, 945–954, https://doi.org/10.5194/angeo-29-945-2011, 2011.

WDC: Geomagnetic Equatorial Dst index Home Page, available at: http://wdc.kugi.kyoto-u.ac.jp/dstdir/, last access: June 2020.

Weimer, D. R.: An improved model of ionospheric electric potentials including substorm perturbations and application to the Geospace Environment Modeling November 24, 1996, event, J. Geophys. Res.-Space, 106, 407–416, https://doi.org/10.1029/2000JA000604, 2001.

Yau, A. W., Shelley, E. G., Peterson, W. K., and Lenchyshyn, L.: Energetic auroral and polar ion outflow at DE 1 altitudes: Magnitude, composition, magnetic activity dependence, and long-term variations, J. Geophys. Res.-Space, 90, 8417–8432, https://doi.org/10.1029/JA090iA09p08417, 1985.

Yau, A. W., Peterson, W. K., and Shelley, E. G.: Quantitative Parametrization of Energetic Ionospheric Ion Outflow, in: book series Geophysical Monograph Series, Modeling Magnetospheric Plasma, Vol. 44, American Geophysical Union (AGU), Washington, D.C., 211–217, https://doi.org/10.1029/GM044p0211, 1988.

Yau, A. W., Abe, T., and Peterson, W.: The polar wind: Recent observations, J. Atmos. Sol.-Terr. Phy., 69, 1936–1983, https://doi.org/10.1016/j.jastp.2007.08.010, 2007.